Acta Neuropathologica (2023) 145:717–731
https://doi.org/10.1007/s00401-023-02559-z

ORIGINAL PAPER

Physiological β-amyloid clearance by the liver and its therapeutic potential for Alzheimer's disease

Yuan Cheng[1,2,3,4,5] · Chen-Yang He[1,2,3,6] · Ding-Yuan Tian[1,7] · Si-Han Chen[1,2,3] · Jun-Rong Ren[1,2,3] · Hao-Lun Sun[1,8] · Man-Yu Xu[1,2,3] · Cheng-Rong Tan[1,2,3] · Dong-Yu Fan[1,8] · Jie-Ming Jian[1,2,3] · Pu-Yang Sun[1,2,3] · Gui-Hua Zeng[1,2,3] · Ying-Ying Shen[1,2,3] · An-Yu Shi[1,2,3] · Wang-Sheng Jin[1,2,3] · Xian-Le Bu[1,2,3] · Hong-Ming Liu[9] · Yu-Ming Xu[10] · Jun Wang[1,2,3] · Yan-Jiang Wang[1,2,3,11,12,13]

Received: 9 January 2023 / Revised: 8 March 2023 / Accepted: 9 March 2023 / Published online: 25 March 2023

Abstract

Cerebral amyloid-β (Aβ) accumulation due to impaired Aβ clearance is a pivotal event in the pathogenesis of Alzheimer's disease (AD). Considerable brain-derived Aβ is cleared via transporting to the periphery. The liver is the largest organ responsible for the clearance of metabolites in the periphery. Whether the liver physiologically clears circulating Aβ and its therapeutic potential for AD remains unclear. Here, we found that about 13.9% of Aβ42 and 8.9% of Aβ40 were removed from the blood when flowing through the liver, and this capacity was decreased with Aβ receptor LRP-1 expression down-regulated in hepatocytes in the aged animals. Partial blockage of hepatic blood flow increased Aβ levels in both blood and brain interstitial fluid. The chronic decline in hepatic Aβ clearance via LRP-1 knockdown specific in hepatocytes aggravated cerebral Aβ burden and cognitive deficits, while enhancing hepatic Aβ clearance via LRP-1 overexpression attenuated cerebral Aβ deposition and cognitive impairments in APP/PS1 mice. Our findings demonstrate that the liver physiologically clears blood Aβ and regulates brain Aβ levels, suggesting that a decline of hepatic Aβ clearance during aging could be involved in AD development, and hepatic Aβ clearance is a novel therapeutic approach for AD.

Keywords Alzheimer's disease · β-Amyloid · Liver · LRP-1 · Clearance

Yuan Cheng and Chen-Yang He these authors contributed equally.

✉ Yu-Ming Xu
xuyuming@zzu.edu.cn

✉ Jun Wang
qywangjun@163.com

✉ Yan-Jiang Wang
yanjiang_wang@tmmu.edu.cn

1 Department of Neurology and Centre for Clinical Neuroscience, Daping Hospital, Third Military Medical University, Chongqing, China

2 Institute of Brain and Intelligence, Third Military Medical University, Chongqing, China

3 Chongqing Key Laboratory of Ageing and Brain Diseases, Chongqing, China

4 Department of Neurology and Institute of Neurology, Huashan Hospital, State Key Laboratory of Medical Neurobiology and MOE Frontiers Center for Brain Science, Shanghai Medical College, Fudan University, Shanghai, China

5 National Center for Neurological Disorders, Shanghai, China

6 Department of Neurology, The General Hospital of Western Theater Command, Chengdu 610000, China

7 Department of Cardiology, Southwest Hospital, Third Military Medical University, Chongqing, China

8 Shigatse Branch, Xinqiao Hospital, Third Military Medical University, Shigatse, China

9 Department of Hepatobiliary Surgery, Daping Hospital, Third Military Medical University, Chongqing, China

10 Department of Neurology, The First Affiliated Hospital of Zhengzhou University, Zhengzhou University, Zhengzhou, Henan, China

11 Chongqing Institute for Brain and Intelligence, Guangyang Bay Laboratory, Chongqing, China

12 Center for Excellence in Brain Science and Intelligence Technology, Chinese Academy of Sciences, Shanghai, China

13 State Key Laboratory of Trauma, Burns, and Combined Injury, Third Military Medical University, Chongqing, China

Introduction

Alzheimer's disease (AD) is the most common type of dementia, and few disease-modifying treatments are available to halt or slow its progression to date. Cerebral β-amyloid (Aβ) accumulation is a pivotal event in the pathogenesis of AD [12]. Impairment of Aβ clearance is considered the main cause of sporadic AD, which accounts for 99% of all AD cases [29]. Recently, two disease-modifying drugs, aducanumab and lecanemab, have shown beneficial efficacy in phase 3 trials in patients with early AD, and have been approved for the treatment of AD [1, 3, 38]. The breakthrough of Aβ antibodies in clinical trials suggests that Aβ clearance is an effective way to prevent and treat AD, and also indicates the critical role of Aβ clearance dysfunction in AD pathogenesis. Therefore, understanding the mechanism of Aβ clearance from the brain could be crucial to establish interventions for AD [14, 28].

AD is traditionally considered a disease of the brain itself. However, the pools of Aβ in the brain and the periphery communicate with each other [39]. Approximately 40–60% of brain-derived Aβ is cleared through transport into the periphery via the blood–brain barrier, glymphatic–lymphatic pathway, etc. [25, 42]. However, where and how brain-derived Aβ peptides are cleared in the periphery remains unclear.

The liver is the largest organ responsible for clearing metabolites from the blood [9, 11]. Hepatic dysfunction is linked to both cognitive decline and AD in humans [22, 23]. A genome-wide meta-analysis indicates that some AD-associated risk genes, such as *APOE, CLU, ABCA7,* etc., are highly expressed in liver cells [15]. These findings suggest that the liver might play a critical role in Aβ clearance and AD pathogenesis. This study aimed to investigate the physiological function of the liver in clearing Aβ from the blood and its role in regulating brain Aβ deposition and to explore the therapeutic potential of liver-mediated Aβ clearance for AD.

Materials and methods

Subjects

This study was approved by the Institutional Review Board of Daping Hospital, Third Military Medical University, Chongqing, China. To investigate the impact of liver aging on Aβ clearance, 84 cognitively normal subjects aged from 40 to 90 years, whose data on blood Aβ and hepatic function were available, were enrolled from the Chongqing Ageing and Dementia Study (CADS) cohort. To observe the impact of liver disease on Aβ clearance, 53 patients with liver cirrhosis and 38 age- and gender-matched controls with normal hepatic function were included from Daping Hospital (Supplementary Table 1). Subjects were excluded from the study if they had severe cardiac, pulmonary, or kidney diseases, tumors, or experienced cerebral vascular events or complaints of cognitive dysfunction. The hepatic function indexes were extracted from the case system, including serum total bilirubin (TBIL), alanine aminotransferase (ALT), aspartate aminotransferase (AST), and ALT/AST ratio.

Animals

All these procedures in the present study were approved by the Animal Ethics Committee of Third Military University (Ethics Approval ID: AMUWEC20191346). APPswe/PS1dE9 transgenic (Tg) mice on a C57BL/6 background and C57BL/6 wild type (WT) mice were obtained from the Jackson Laboratory (Allele Symbol: B6.Cg-Tg(APPswe,PSEN1dE9)85Dbo/Mmjax, RRID:MMRRC_034832-JAX) and bred in the animal facility of Daping Hospital. Female mice were used in our study to eliminate the potential impacts of sex on AD pathologies.

Three-month-old female rabbits were used to investigate the differences in Aβ levels between hepatic inflow and outflow blood. Three-, 6-, 18-, and 36-month-old female rabbits were used to explore the change in hepatic Aβ clearance with aging. Five milliliters of blood was collected from the hepatic artery, portal vein, and posterior vena cava vein. Sixty percent of Aβ in the portal vein and 40% of Aβ in the hepatic artery were considered to constitute the total Aβ amount in liver inflow blood, and the Aβ level difference between the posterior vena cava vein before and after converging with the liver vein was considered to be the total Aβ amount in liver outflow blood in the present study [4, 7]. The plasma was separated immediately after blood collection.

Parabiosis

To demonstrate Aβ uptake by the liver, we selected 6- to 9-month-old APPswe/PS1dE9 transgenic (Tg) mice and their age- and weight-matched WT littermates ($n=3$ in each group) on a C57BL/6 background to establish a parabiosis model following our previous study [43]. All the mice were bred in the animal facility of Daping Hospital. All mouse husbandry procedures were approved by the Third Military Medical University Animal Welfare Committee. Female Tg mice were used in this parabiosis experiment to exclude the influence of sex on brain Aβ deposition. Each pair of mice was placed together in a cage for 1 month to allow the mice to adapt to each other. Female Tg mice and their age- and weight-matched female WT littermates were

selected for parabiosis from 6 months of age to 9 months of age ($n=3$ per group). The parabiosis surgery was conducted as described in a previous study [43]. Briefly, animals were anesthetized and placed in a parallel orientation. A left lateral incision was made on one mouse, while a right incision was made on the partner mouse, extending from the base of the ear towards the hip. The incision included skin and muscle along the thorax and abdomen. The opposing muscle layers of the two mice were joined with 5–0 silk sutures. The scapulae of the mice were fixed together with 4–0 silk sutures. The corresponding dorsal and ventral skin was sutured with 4–0 silk. After the surgery, the parabiotic mice were allowed to recover in a warm and clean environment before being transferred into the husbandry area. Prophylactic antibiotic treatment (enrofloxacin, 5 mg/kg) was started 1 day before the surgery and continued for 1 week. All animals received analgesic/anti-inflammatory treatment (acetylsalicylic acid 5 mg/kg) for 2 weeks.

Hepatic portal vein ligation and microdialysis

Six-month-old AD mice were subjected to hepatic portal vein ligation (PVL) and microdialysis experiments ($n=5$ in each group). Microdialysis was performed as previously described [19]. In brief, a guide cannula (Microbiotech se/AB, Sweden) was stereotactically implanted in the right hippocampus (A/P: − 2.0 mm, M/L: 2.0 mm, D/V: − 2.0 mm) and fixed using binary dental cement. After a recovery period of at least 7 days, PVL surgery was conducted. Briefly, surgical procedures were conducted under inhalation anesthesia consisting of a mixture of 3% isoflurane and pure oxygen at a flow rate of 0.5 L/min (RWD Life Science Co., Ltd., China). Following skin disinfection, the abdominal cavity was opened via a transverse upper abdominal incision. The intestine was removed and covered by wet gauze. Portal vein branches were dissected from the artery and bile duct and then ligated with surgical sutures using an operating microscope. Then, a probe with a 100 kDa cutoff (Microbiotech se/AB, Sweden) was inserted through the guide cannula. The probe was connected to a microdialysis peristaltic pump (CMA, Sweden), which was operated in push–pull mode. Artificial cerebral spinal fluid (ACSF) containing 4% human albumin solution was introduced at a flow rate of 1 µL/min for interstitial fluid (ISF) collection.

In vivo optical near-infrared imaging of liver Aβ uptake

Three-month-old mice were used to detect hepatic Aβ40 and Aβ42 distribution over time ($n=3$). Three- and 15-month-old mice were used to investigate the changes in fluorescence intensity in the liver area with aging ($n=3$ in each group). Mice underwent surgical abdominal skin preparation and fasted 24 h in advance to avoid fluorescent signal interference by hair and fodder. Cy5.5-labeled Aβ (200 µL, 1 ng/mL) (RuiXiBio, Xian, China) was administered to mice via tail vein injection. Then, the fluorescence intensity of the liver area in the upper right abdomen of mice was dynamically detected every 2 h. Near-infrared imaging was performed on an IVIS® Lumina III In Vivo Imaging System (PerkinElmer, USA). The data were analyzed by IVIS Living Image Software. All parameters consist of photo adjustment, and individual image color scales are consistent.

Primary hepatocyte isolation and flow cytometry

For evaluation of hepatocyte Aβ uptake capacity with age, primary hepatocytes of 3- and 15-month-old mice ($n=5$ in each group) were isolated as previously reported [5, 31]. The liver was washed by perfusion, and hepatocytes were dissociated by collagenase, separated from other cells, and cultured with FITC-labeled Aβ42 (GL Biochem (Shanghai), Ltd.) for flow cytometry. In brief, the livers of APP/PS1 mice were first perfused with calcium and magnesium-free Hank's balanced salt solution containing 10 nM Ethylene Glycol Tetraacetic Acid (EGTA) and 10 nM *N*-2-hydroxyethylpiperazine-*N*-2-ethanesulfonic acid (HEPES) at 5 mL/min for 10 min. The liver was sequentially perfused with low-glucose DMEM containing 25 µg/mL Liberase (Liberase™ Research Grade, Sigma-Aldrich, USA) at 5 mL/min. All perfusion solutions were preheated and maintained at 37 °C before use.

Then, the liver was dissected gently, the gallbladder was removed, and the liver was placed in a dish with low-glucose DMEM. The liver sack was ruptured with fine tip forceps in a few locations along the liver surface, and the cells were gently released and centrifuged at 50*g* for 2 min. The supernatant was aspirated, 5 mL of low-glucose DMEM containing 10% fetal bovine serum (FBS) was added, and the cells were resuspended by swirling the tube. The cell suspension was mixed with CD45 and CD146 microbeads. The CD45 antigen is expressed on all cells of hematopoietic origin except erythrocytes and platelets, and the CD146 antigen has been developed to isolate mouse liver sinusoidal endothelial cells (LSECs). The CD45(−) CD146(−) cells removed from the total cell suspension were regarded as hepatocytes. Then, the mixed cell suspension was loaded onto a MACS® Column, which was placed in the magnetic field of a MACS separator. The magnetically labeled CD45(+) and CD146(+) cells were retained on the column. The unlabelled cells ran through, and this cell fraction was depleted of CD45(+) and CD146(+) cells and were considered hepatocytes [21].

Isolated hepatocytes were resuspended in low-glucose DMEM with 10% FBS and 1% penicillin/streptomycin and adjusted to a concentration of 2×10^6 cells/mL. For analysis of the uptake of Aβ, hepatocytes were incubated with

FITC-Aβ42 (1 μg/mL) (GL Biochem, Shanghai, China) for 1 h at 37 °C in a 5% CO_2 incubator. Following incubation, the cell suspensions were discarded, and adherent cells were detached from the well plate with 0.25% trypsin and washed with fluorescence-activated cell sorting (FACS) buffer twice fixed with 1% paraformaldehyde. Flow cytometry was performed on a NovoCyte Flow Cytometer (Beckman Coulter, CA, USA). The data were analyzed by the CytExpert software based on forward and side scatter and the mean fluorescence intensity. For consistent testing conditions, a gating strategy was designed and applied equivalently across all study samples.

Liver-specific LRP-1 knockdown and adeno-associated virus (AAV)-mediated expression of the mini LRP-1 gene (mLRP-1) in the liver

To investigate the chronic impacts of damaged liver Aβ clearance on brain AD-related pathologies, we injected 3-month-old APP/PS1 mice with liver-specific LRP-1 knockdown virus [rAAV2/8-hTBG-shRNA(Lrp1)-eGFP-WPRE-pA] and control virus [rAAV2/8-hTBG-shRNA(scramble)-eGFP-WPRE-pA] (BrainVTA, China) via the tail vein, and mice were sacrificed and analyzed at 9 months of age ($n=9$ in each group). In addition, to determine the treatment effect of enhanced liver LRP-1-mediated Aβ clearance, the previously reported LRP-1 minigene (mLRP-1) containing the LRP-IV extracellular domain and the intracellular cytoplasmic domain of the LRP-1 gene was packaged into liver-specific AAV vector particles [24], and 6-month-old APP/PS1 mice subjected to virus (AAV2/8-hTBG-Lrp1_mini_DomIV-3HA-pA) and (AAV2/8-hTBG-eGFP-WPRE-pA) injection (Taitool Bioscience, China) were sacrificed and analyzed at 12 months of age ($n=7$ in each group). The plasmid information of the LRP-1 minigene was kindly provided by Dr. Berislav V. Zlokovic at Zilkha Neurogenetic Institute, University of Southern California.

Brain sampling

The brains were sampled and weighed. The right hemispheres were fixed in 4% paraformaldehyde (pH 7.4) at 4 °C for 24 h and then incubated with 30% sucrose for 48 h. The left hemispheres were snap-frozen in liquid nitrogen and stored at − 80 °C for future biochemical analysis.

AD pathologies and quantification

Brain sections were cut coronally at a thickness of 30 μm and stored at − 20 °C in PBS with 0.1% sodium azide. A series of five isometric brain sections (~ 1.3 mm apart) were used for each staining protocol. Congo red staining and immunohistochemistry with a 6E10 antibody (803008, BioLegend, USA) were used to identify compact and total Aβ plaques as previously described. Each isometric brain section containing the hippocampus was used. Apoptosis or damage of neuronal cells was assessed using double immunofluorescence staining for NeuN (ab104224, Abcam, UK) and cleaved Caspase-3 (ab13847, Abcam, UK). Neuronal degeneration was detected using double immunofluorescence staining with a NeuN and microtubule-associated protein (MAP)-2 antibody (ab183830, Abcam, UK). Immunohistochemistry with an anti-CD68 antibody (ab125212, Abcam, UK) was used to detect microglia. Astrocytes were detected by immunohistochemistry with an anti-glial fibrillary acidic protein (GFAP) antibody (ab134436, Abcam, UK). Phosphorylated tau was detected by immunohistochemical staining with a PT231 antibody (Peptide epitope: aa. 229–233 (V-R-T-P-P) derived from Human Tau.) (21099, Signalway Antibody, USA). The area fraction and/or density of positive staining and the number of cells were quantified with ImageJ software in a blinded manner.

Quantification of dendrite spines by Golgi staining

Golgi staining was performed according to the manufacturer's protocols (Hito Golgi-Cox OptimStain™ kit, USA). The numerical density of spines was assessed in CA1 pyramidal neurons. The number of dendritic spines was estimated at high magnification (1000×) in a blinded manner. Pyramidal neurons were chosen from three visual fields scattered in CA1 region in each brain slice, and three consecutive brain slices containing the CA1 region were selected from each mouse.

Immunohistochemical and immunofluorescence analysis of the liver

A series of 8-μm sections of mouse liver and 8-μm sections from human liver punctures were subjected to immunohistochemistry with a MOAB-2 antibody (6C3, MABN254, Sigma, USA), which only recognizes Aβ fibers and oligomers but not the APP protein, and then counterstained with hematoxylin (H-3401, Vector Laboratories) to detect nuclei. The tissue-specific distribution of Aβ in the liver was detected by double immunofluorescence staining with a MOAB-2 antibody and an albumin antibody (SAB3500217, Sigma, USA) and then mounted onto slides with a DAPI fluorescence mounting medium (Dako). All immunofluorescence-stained sections were imaged with a Zeiss LSM 900 confocal laser-scanning microscope (Germany) using a series of high-resolution optical sections (1024 × 1024-pixel format). Laser settings for gain, digital offset, and laser intensity were kept standardized between different samples.

ELISA

Human plasma Aβ40 and Aβ42 levels were measured using an enzyme-linked immunosorbent assay (ELISA) kit (Invitrogen, USA) according to the manufacturer's instructions. Frozen mouse brain samples were weighed, pulverized in liquid nitrogen, and sequentially extracted in Tris buffer solution (TBS), 2% sodium dodecyl sulfonate (SDS), and 70% formic acid (FA). The levels of Aβ40 and Aβ42 in brain extracts, blood, and bile were measured using supersensitive ELISA kits (Invitrogen, USA). The levels of the proinflammatory cytokines TNF-α, IFN-γ, IL-1β, and IL-6 and the anti-inflammatory cytokines IL-4 and IL-10 in brain homogenates and the blood were measured using ELISA kits (eBioscience, USA). The levels of alanine aminotransferase (ALT), aspartate aminotransferase (AST), and soluble LRP-1 (sLRP-1) in plasma were measured using ELISA kits (Jiangsu Jingmei Biotechnology Co., Ltd., China). The levels of cholesterol in the brain and plasma were measured using ELISA kits (Sigma, USA).

Western blotting

Proteins were extracted from brain homogenates in RIPA buffer. The samples were separated on SDS-PAGE (4–20% acrylamide) gels and transferred to nitrocellulose membranes. The blots were probed with the following primary antibodies: an anti-insulin-degrading enzyme (IDE) antibody (ab32216, Abcam, UK), an anti-neprilysin (NEP) antibody (AB5458, Millipore, USA), anti-low density lipoprotein receptor-related protein 1 (LRP-1) (ab92544, Abcam, UK), anti-HA-Tag (C29F4, Cell Signaling Technology, USA), anti-Cathepsin-D (ARG55566, Arigo, China), anti-Cathepsin-S (ARG40174, Arigo, China), anti-Lamp-1 (ab62562, Abcam, UK), anti-Lamp-2a (ab18528, Abcam, UK), an anti-PSD95 antibody (MABN68, Merck, USA), an anti-Synapsin-1 antibody (MABN894, Merck, USA), an anti-SNAP-25 antibody (MAB331-C, Merck, USA), an anti-GAPDH antibody (G9545, Sigma, USA), and a β-actin antibody (A1978, Sigma, USA). The membranes were incubated with secondary antibodies conjugated to IRDye 800CW (Invitrogen, USA) and scanned with an Odyssey fluorescence scanner. The band density was normalized to that of brain β-actin or liver GAPDH for analysis.

Behavioral tests

Mice were subjected to behavioral tests, including the Y-maze test, open-field test, and Morris water maze test, as previously described [44]. In brief, mice were allowed to move freely through a Y-maze for 5 min for the spontaneous alternation test. Entry into all three arms in an overlapping triplet set was defined as a successive alternation. In the novel arm exploration test, the mice were allowed to explore the home arm and familiar arm in the Y-maze for 5 min, with the novel arm blocked. After a 30-min interval, the mice were allowed to freely explore all the arms for 5 min. Novel arm entries and time spent in the novel arm were recorded. In the open-field test, each mouse was placed in the center of the apparatus for 5 min. Rearing, grooming, defecation, and urination were recorded, and the paths and distance traveled were recorded using a computer tracking system with ANY-maze software (Stoelting, USA). The swimming abilities of the mice were tested before the Morris water maze test. Then, each mouse was trained daily on three platform trials for 5 consecutive days, after which a probe trial was performed. Performance was recorded and analyzed with ANY-maze software (Stoelting, USA).

Statistical analysis

The data are expressed as the mean ± SEM. All analyses were completed using SPSS 20.0 software (Chicago, USA). Comparisons between two groups were made by two-tailed Student's *t* test or paired *t* test as deemed appropriate. Comparisons among multiple groups were made by one-way ANOVA followed by the least significant difference (LSD) test. Normality and equal variance tests were performed for all assays. A p value < 0.05 was considered statistically significant. Analyses in this study were performed in a blinded manner. All figures were plotted using GraphPad Prism software (San Diego, USA).

Results

The liver physiologically clears circulating Aβ

We observed Aβ-positive staining in the hepatocytes of both humans and APP/PS1 mice with different antibodies to Aβ, such as 6C3 antibody which only detects Aβ but not full-length APP protein (Fig. 1a, b), OC antibody which detects Aβ in various aggregation species, as well as 6E10 antibody which detects Aβ peptides and the abundant full-length APP protein (Supplementary Fig. 1). Then, using the parabiosis model of APP/PS1 mice and wild type (WT) mice, we detected high levels of human Aβ40 and Aβ42 in the liver homogenates of the parabiotic WT mice (paraWT) mice, suggesting that human Aβ in circulating blood produced by the parabiotic APP/PS1 (paraAPP/PS1) mice was physiologically taken up by the liver of the paraWT mice (Fig. 1c). Additionally, via near-infrared imaging in vivo, we observed that intravenously injected Cy5.5-labeled Aβ42 existed in the liver, and the fluorescence intensity in the liver gradually decreased after reaching a peak at 4–7 h, confirming that the liver takes up and clears Aβ from the blood (Fig. 1d).

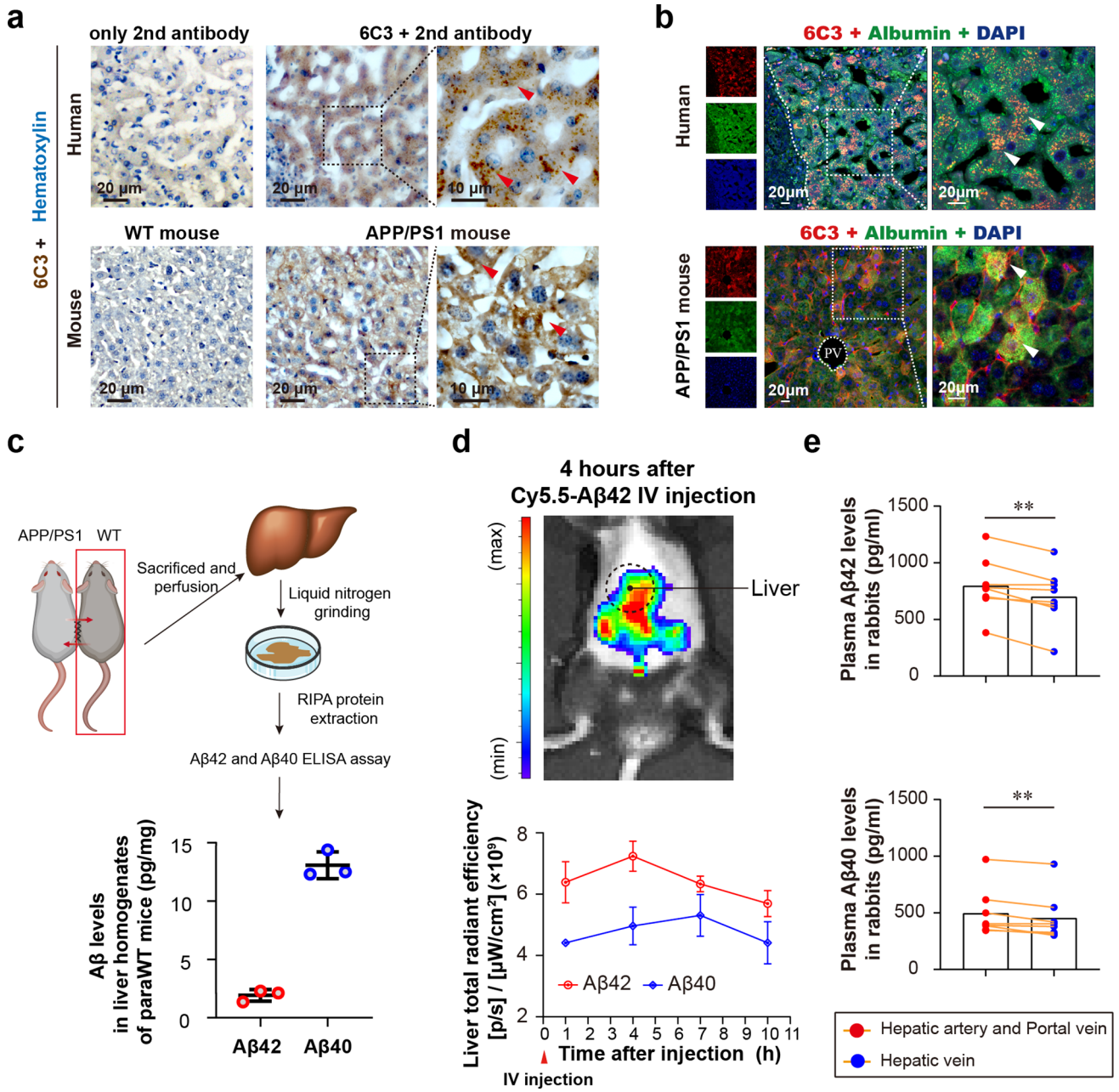

Fig. 1 Physiological Aβ clearance of the liver. **a** Immunohistochemical staining of the livers of humans with or without anti-Aβ antibody (6C3) and immunohistochemical staining of the livers of APP/PS1 mice and WT mice. **b** Representative confocal images of Aβ exist in the livers of humans and APP/PS1 mice, as detected by immunofluorescence staining with antibodies against albumin (green) and Aβ (red), and DAPI (blue). The arrows indicate Aβ staining within the hepatocytes. **c** Measurement of Aβ in the livers of the paraWT mice in a parabiosis model. Both Aβ42 and Aβ40 could be detected by ELISAs ($n=3$). **d** The distribution and dynamic changes of Cy5.5-labeled Aβ42 and Aβ40 in the hepatic region over time via near-infrared imaging in vivo. **e** Comparison of Aβ levels in the liver outflow and inflow blood of rabbits. Paired *t* test, $n=8$ per group. $^{*}p<0.05$, $^{**}p<0.01$, $^{***}p<0.001$. The error bars represent the SEMs. *Aβ* amyloid-β protein, *IV* intravenous, *PV* portal vein

Then, we measured Aβ levels in the hepatic inflow (composites of hepatic artery and portal vein) and outflow blood (hepatic vein) in rabbits to assess the capacity of the liver in clearing circulating Aβ. The results showed that the Aβ42 and Aβ40 levels in hepatic outflow blood were 13.9% and 8.9% lower, respectively, than those in inflow blood (Fig. 1e), suggesting that circulating Aβ is removed when flowing through the liver.

The above findings indicate that the liver physiologically clears Aβ from the blood.

Partial blockage of hepatic blood flow increases Aβ levels in blood and brain in APP/PS1 mice

We then examined the impact of the hepatic Aβ clearance on blood and brain Aβ levels. Firstly, we found that plasma Aβ40 and Aβ42 levels were increased in patients with liver cirrhosis compared with controls with normal hepatic function (Supplementary Fig. 2). Then, in 6-month-old APP/PS1 mice, the hepatic portal vein was ligated to partially block hepatic inflow blood and thus to decrease Aβ clearance by the liver. Blood Aβ42 and Aβ40 levels were increased 7.1-fold and 2.9-fold respectively at 6 h after portal vein ligation (Fig. 2a, b). Importantly, Aβ42 and Aβ40 levels in the interstitial fluid (ISF) of the brain were also elevated 1.5-fold and 1.2-fold respectively in parallel with the increase of circulating Aβ (Fig. 2c, d). These results suggest that the liver plays a critical role in regulating the dynamics of Aβ levels in both the blood and the brain.

The capacity of Aβ clearance by the liver declines with age

We investigated the changes in the capacity of Aβ clearance by the liver in aging. Cy5.5-labeled Aβ42 peptides were intravenously injected in young (3-month-old) and aged (15-month-old) APP/PS1 mice. We found that the maximum fluorescence intensity in the liver area was lower and the peak arrival time was longer in the aged mice than in the young mice (Fig. 3a–c). There were no differences between the two groups after injection of Cy5.5-labeled reversed Aβ42 peptide (Fig. 3b, d). In addition, we compared the ratio of Aβ concentrations in liver outflow and inflow blood ($Q_{out/in}$) in rabbits of different ages and found increased $Q_{out/in}$ of Aβ40 and Aβ42 in the aged rabbits compared with the young rabbits (Fig. 3e). When comparing the concentration ratio of Aβ in the liver outflow and hepatic artery ($Q_{out/ha}$) and portal vein blood ($Q_{out/pv}$), consistent results were obtained (Supplementary Fig. 3a, b). Next, the hepatocytes of young and aged mice were isolated and coincubated with FITC-labeled Aβ42 peptides (Fig. 3f). The total fluorescence intensity and the percentage of FITC-positive hepatocytes were lower in the aged mice than in the young mice (Fig. 3g, h). These in vivo and in vitro results consistently indicate that the capacity of Aβ clearance by the liver declines with age. Then we examined the impact of the age-related decrease in Aβ clearance by the liver on blood Aβ levels. As expected, we observed an increase in blood Aβ40 and Aβ42 levels in the aged rabbits than the young ones

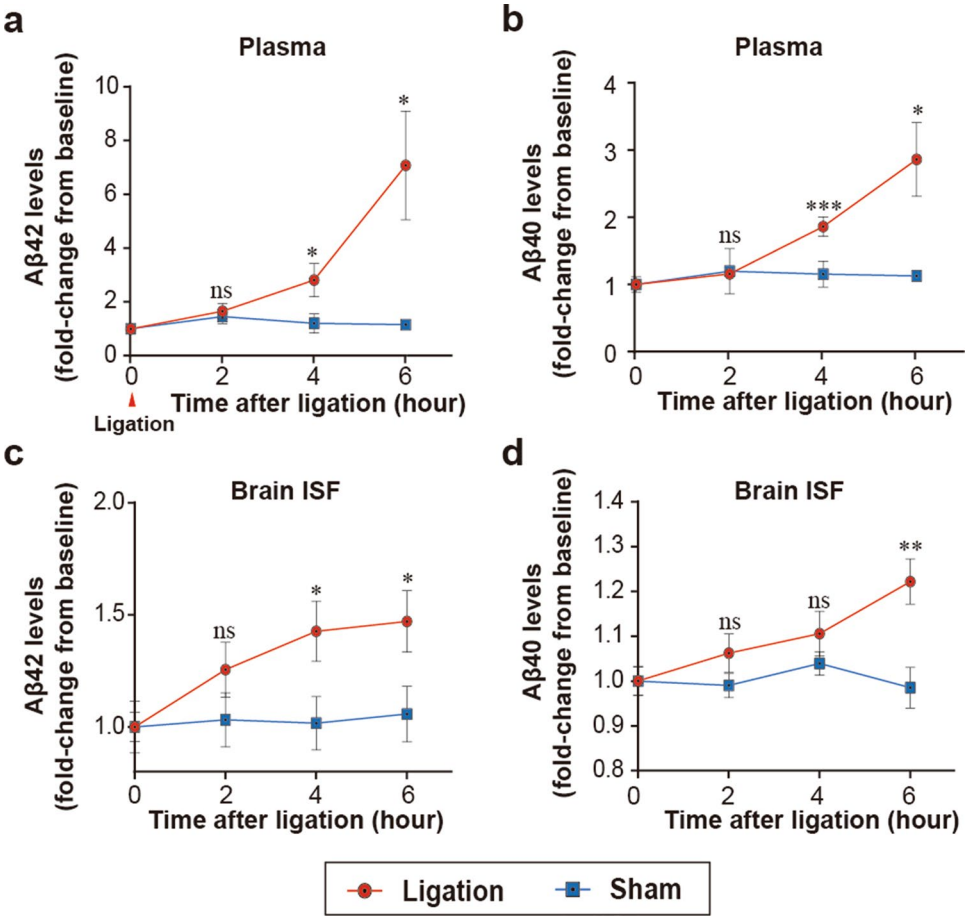

Fig. 2 Liver portal vein ligation increases Aβ levels in the blood and brain in APP/PS1 mice. **a**, **b** Levels of Aβ42 and Aβ40 in the plasma of APP/PS1 mice before and after liver portal vein ligation. **c**, **d** Levels of Aβ42 and Aβ40 in the ISF of APP/PS1 mice before and after liver portal vein ligation. Unpaired *t* test, $n = 5$ per group. $^{*}p < 0.05$, $^{**}p < 0.01$, $^{***}p < 0.001$. ns denotes no significance. The error bars represent the SEMs. *Aβ* amyloid-β protein, *ISF* interstitial space fluid

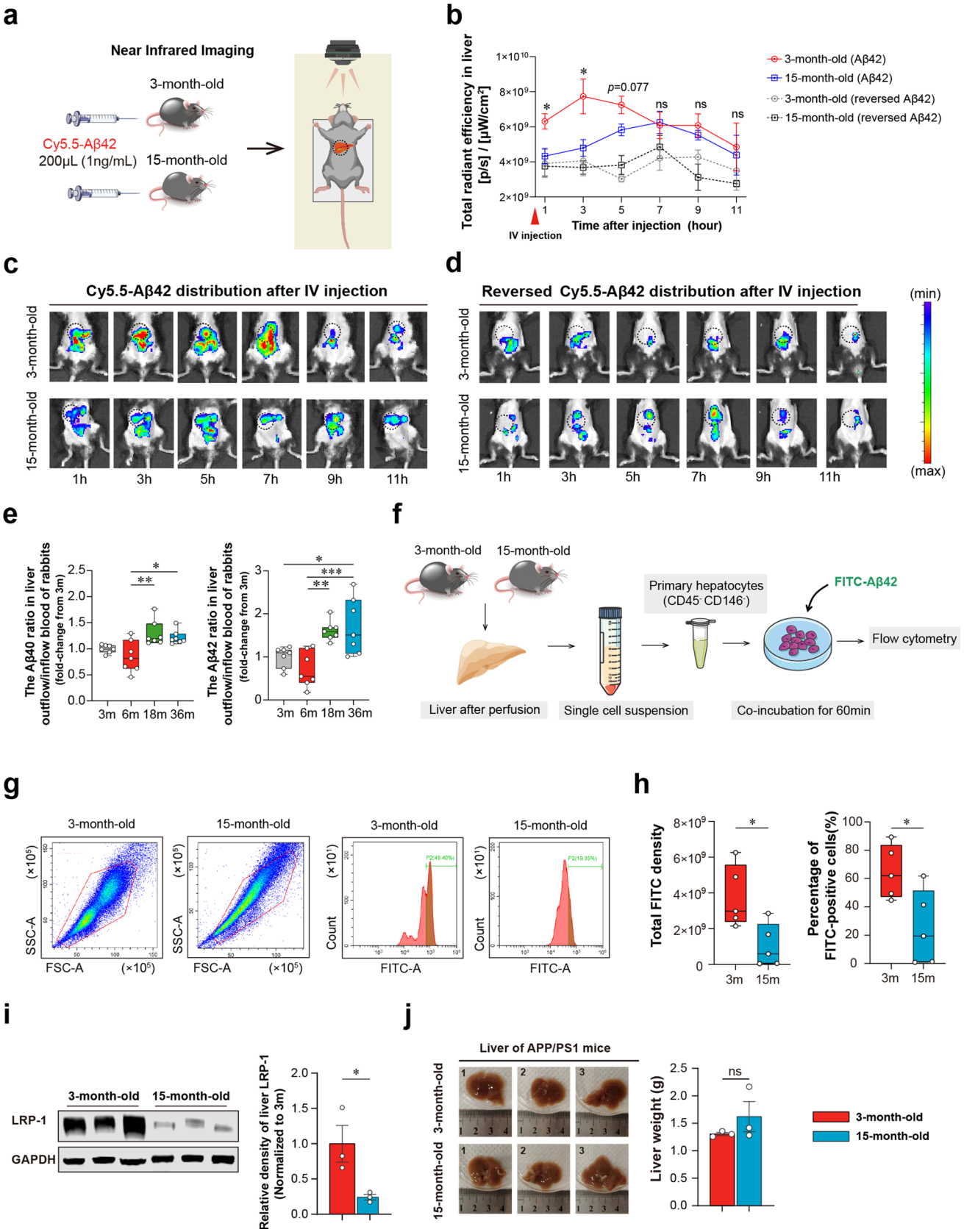
a
Near Infrared Imaging
3-month-old
Cy5.5-Aβ42
200μL (1ng/mL)
15-month-old
b
Total radiant efficiency in liver [p/s] / [μW/cm²]
1×10¹⁰
8×10⁹
6×10⁹
4×10⁹
2×10⁹
p=0.077
ns
IV injection
Time after injection (hour)
3-month-old (Aβ42)
15-month-old (Aβ42)
3-month-old (reversed Aβ42)
15-month-old (reversed Aβ42)
c
Cy5.5-Aβ42 distribution after IV injection
3-month-old
15-month-old
1h
3h
5h
7h
9h
11h
d
Reversed Cy5.5-Aβ42 distribution after IV injection
(min)
(max)
e
The Aβ40 ratio in liver outflow/inflow blood of rabbits (fold-change from 3m)
The Aβ42 ratio in liver outflow/inflow blood of rabbits (fold-change from 3m)
3m 6m 18m 36m
f
3-month-old
15-month-old
Primary hepatocytes (CD45⁻CD146⁻)
FITC-Aβ42
Flow cytometry
Liver after perfusion
Single cell suspension
Co-incubation for 60min
g
3-month-old
15-month-old
SSC-A
FSC-A
Count
FITC-A
P2(49.40%)
P2(19.35%)
h
Total FITC density
Percentage of FITC-positive cells(%)
3m
15m
i
3-month-old
15-month-old
LRP-1
GAPDH
Relative density of liver LRP-1 (Normalized to 3m)
j
Liver of APP/PS1 mice
3-month-old
15-month-old
Liver weight (g)
ns

◂**Fig. 3** Hepatic capacity of Aβ clearance declines with aging. **a**, **d** The distribution and dynamic changes of Cy5.5-labeled Aβ42 and reversed Aβ42 in the liver region of 3- and 15-month-old mice over time via near-infrared imaging in vivo. Unpaired *t* test, $n=3$ per group. **e** The Aβ ratio of liver outflow to inflow blood in 3-, 6-, 18-, and 36-month-old rabbits. Unpaired *t* test, $n=7$ per group. **f** Schematic diagram of APP/PS1 mouse primary hepatocyte isolation and flow cytometry. **g** Following CD45 and CD146 double-negative selection by magnetic-activated cell sorting, hepatocytes were identified by flow cytometry. For the measurement of Aβ42 uptake by hepatocytes in the two groups, hepatocytes were gated based on FSC-H and SSC-H. **h** Comparison of the capability of Aβ42 uptake by hepatocytes with aging. Unpaired *t* test, $n=5$ per group. **i** Western blot analysis and quantification of the liver LRP-1 levels between 3- and 15-month-old mice, unpaired *t* test, $n=3$ per group. **j** Comparison of the liver mass between 3- and 15-month-old mice, unpaired *t* test, $n=3$ per group. $^{*}p<0.05$, $^{**}p<0.01$, $^{***}p<0.001$. ns denotes no significance. The error bars represent the SEMs. *FSC-H* forward scatter height, *SSC-H* side scatter height, *Aβ* amyloid-β protein, *IV* intravenous

(Supplementary Fig. 3c, d). Consistently, in cognitively normal humans, plasma Aβ42 and Aβ40 levels were increased with aging. Unfortunately, hepatic function indexes were not associated with either age or plasma Aβ levels (Supplementary Table 2).

LRP-1 is the main receptor responsible for Aβ phagocytosis by hepatocytes [32]. We found that LRP-1 levels in the liver homogenates of the aged mice were decreased compared to those in young mice (Fig. 3i and Supplementary Fig. 3e, i), while the weight of the liver had no significant differences between the two groups (Fig. 3j). No differences were observed in the Aβ-degrading enzymes neprilysin (NEP) and insulin-degrading enzyme (IDE), lysosomal-associated proteins Lamp-1 and Lamp-2, or cathepsin-D and cathepsin-S between the young and aged mice (Supplementary Fig. 3e–h). These results suggest that the compromised hepatic Aβ clearance with aging may be attributed to reduced LRP-1 expression.

Decline of hepatic Aβ clearance aggravates the brain Aβ burden in APP/PS1 mice

To test whether decline of hepatic Aβ clearance contributed to AD development, we specifically knocked down LRP-1 expression in hepatocytes of 3-month-old APP/PS1 mice with AAV-mediated delivery of shLPR1 gene under hepatocyte-specific promoter hTGB (AD-AAV$_{shLRP-1}$) (Fig. 4a). This was further confirmed by the hepatocyte-specific expression of the reporter gene enhanced green fluorescence protein (eGFP) (Supplementary Fig. 4a–c). Mice were sacrificed and analyzed at 9 months of age. The AD-AAV$_{shLRP-1}$ mice had 46% lower levels of LRP-1 in the liver (Fig. 4b, c and Supplementary Fig. 4d, e) and 13.9% lower soluble LRP-1 levels in plasma (Supplementary Fig. 4f) than the AD-AAV$_{vehicle}$ controls.

Compared with the AD-AAV$_{vehicle}$ controls, the AD-AAV$_{shLRP-1}$ mice had lower Aβ levels in the liver (Supplementary Fig. 4g) and higher Aβ levels in the blood (Fig. 4d), suggesting that the capacity of the liver in clearing circulating Aβ was decreased. Furthermore, the AD-AAV$_{shLRP-1}$ mice had more Aβ plaques (Fig. 4e, f) and higher Aβ levels in the brain (Fig. 4g, h). In total, a chronic decline of hepatic Aβ clearance via specifically knockdown LRP-1 in hepatocytes resulted in a ~ 37% increase of Aβ plaque in cerebral cortex and a ~ 43% increase in hippocampus of APP/PS1 mice by 6E10 immunostaining.

No differences in transaminase and cholesterol levels were observed between the two groups (Supplementary Fig. 4h, i), suggesting that the increased cerebral amyloidosis was not likely due to hepatocyte damage and abnormal lipid metabolism.

Decline of hepatic Aβ clearance aggravates other AD-type pathologies in APP/PS1 mice

Compared with the AD-AAV$_{vehicle}$ mice, the AD-AAV$_{shLRP-1}$ mice had higher levels of tau phosphorylation at Thr231 (Supplementary Fig. 5a, b). Moreover, the AD-AAV$_{shLRP-1}$ mice had aggravated neuroinflammation, as reflected by more astrogliosis and microgliosis, as well as higher levels of the proinflammatory cytokine IL-6 and lower levels of the anti-inflammatory cytokine IL-4 in the brain (Supplementary Fig. 5c–e). Furthermore, the AD-AAV$_{shLRP-1}$ mice presented aggravated axonal degeneration, neuronal apoptosis and damage, and loss of dendritic spines and synapses in the brain compared with the AD-AAV$_{vehicle}$ mice (Supplementary Fig. 5f–k). The above findings indicate that the decline of hepatic Aβ clearance aggravates tau hyperphosphorylation, neuroinflammation, and neurodegeneration in the brain.

Decline of hepatic Aβ clearance aggravates behavioral deficits in APP/PS1 mice

Compared with the AD-AAV$_{vehicle}$ mice, the AD-AAV$_{shLRP-1}$ mice displayed worse spatial learning as reflected by a longer escape latency in the platform trial, and worse memory consolidation shown by less time in the target quadrant and fewer platform area crossings in the probe trial in Morris water maze (MWM) test (Fig. 4i–k), as well as worse spatial recognition memory as reflected by less time spent in the novel arm and a lower percentage of spontaneous alternations in the Y-maze test (Fig. 4l). In the open field test, no difference in travel distance was observed between two groups, suggesting that the locomotor activity was not altered in the AD-AAV$_{shLRP-1}$ mice (Fig. 4m).

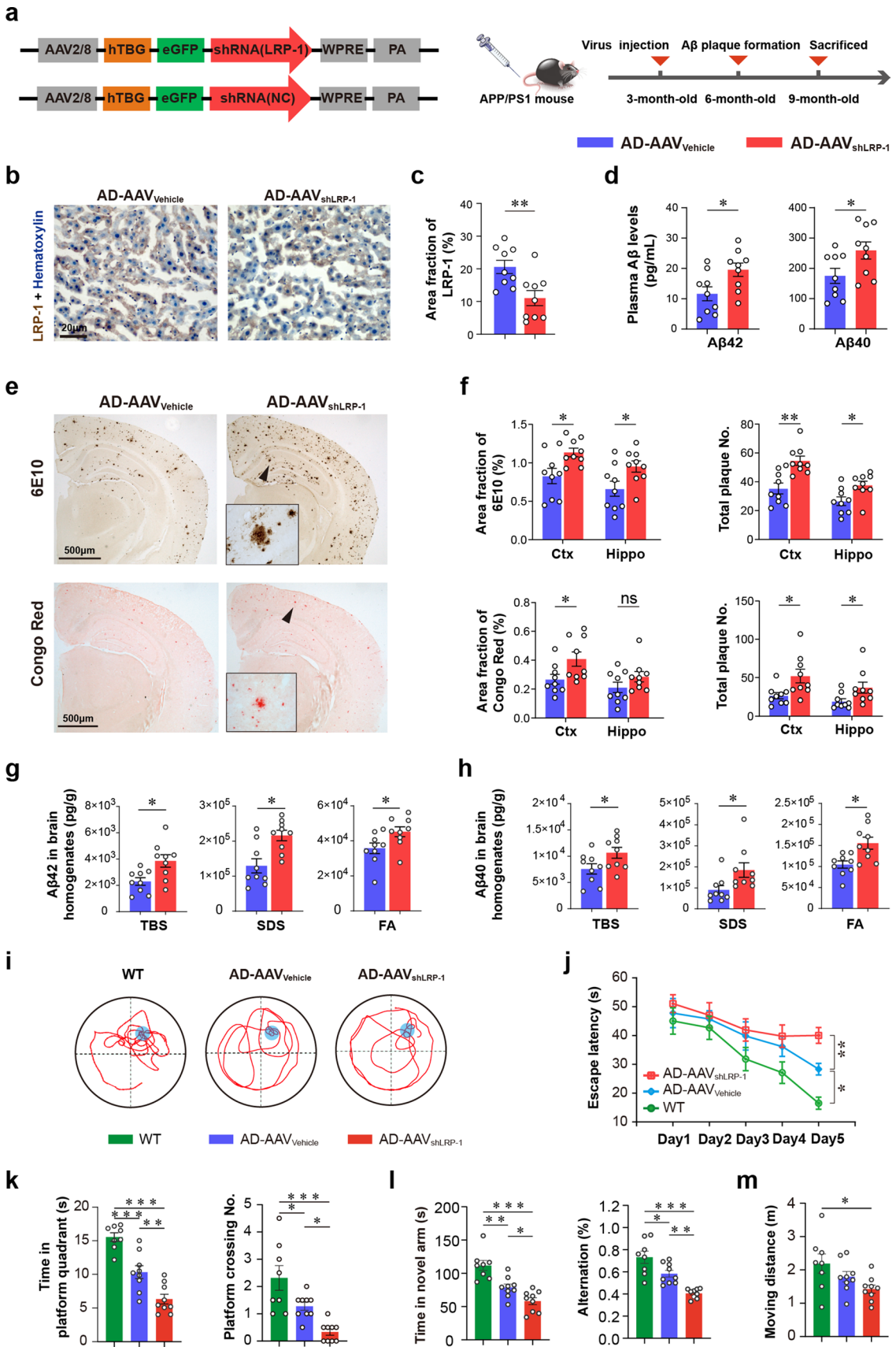
a
AAV2/8 hTBG eGFP shRNA(LRP-1) WPRE PA
AAV2/8 hTBG eGFP shRNA(NC) WPRE PA
APP/PS1 mouse
Virus injection
Aβ plaque formation
Sacrificed
3-month-old
6-month-old
9-month-old
AD-AAVVehicle
AD-AAVshLRP-1
b
LRP-1 + Hematoxylin
20μm
c
Area fraction of LRP-1 (%)
d
Plasma Aβ levels (pg/mL)
Aβ42
Aβ40
e
6E10
Congo Red
500μm
f
Area fraction of 6E10 (%)
Total plaque No.
Area fraction of Congo Red (%)
Ctx
Hippo
ns
g
Aβ42 in brain homogenates (pg/g)
TBS
SDS
FA
h
Aβ40 in brain homogenates (pg/g)
i
WT
j
Escape latency (s)
Day1 Day2 Day3 Day4 Day5
k
Time in platform quadrant (s)
Platform crossing No.
l
Time in novel arm (s)
Alternation (%)
m
Moving distance (m)

◂**Fig. 4** Chronic hepatic dysfunction of Aβ clearance aggravates the brain Aβ burden and cognitive impairments in APP/PS1 mice. **a** Schematic diagram of liver-specific LRP-1 KD virus in a model APP/PS1 mouse (virus injection at 3 months of age and analysis at 9 months of age). **b**, **c** The knockdown effects of the virus, as reflected by immunohistochemical staining with anti-LRP-1 antibody. **d** Aβ levels in the blood of the AD-AAV$_{shLRP-1}$ and AD-AAV$_{vehicle}$ mice. Unpaired *t* test, $n=9$ per group. **e**, **f** Immunostaining and quantification of Aβ plaques stained with 6E10 and Congo red in the neocortex and hippocampus of 9-month-old AD-AAV$_{shLRP-1}$ and AD-AAV$_{vehicle}$ mice. Unpaired *t* test, $n=9$ per group. **g**, **h** Comparison of Aβ42 and Aβ40 levels in the TBS, SDS, and FA fractions of brain homogenates between the AD-AAV$_{shLRP-1}$ and AD-AAV$_{vehicle}$ mice. **i**, **j** Water maze tracing graphs and latency from day one to day five. **k** Time spent in the platform quadrant and platform crossing numbers in the target quadrant by wild type, AD-AAV$_{shLRP-1}$, and AD-AAV$_{vehicle}$ mice in the Morris water maze. One-way ANOVA, $n=8$ in WT group, $n=9$ in AD-AAV group. **l** The time spent in the novel arm, and the percentage of alternations in the Y-maze test. One-way ANOVA, $n=8$ in WT group, $n=9$ in AD-AAV group. **m** Moving distance of wild type, AD-AAV$_{shLRP-1}$, and AD-AAV$_{vehicle}$ mice in the open-field test. One-way ANOVA, $n=8$ in WT group, $n=9$ in AD-AAV group. $^{*}p<0.05$, $^{**}p<0.01$. $^{***}p<0.001$. ns denotes no significance. The error bars represent the SEMs. *Aβ* amyloid-β protein, *TBS* Tris buffer solution, *SDS* sodium dodecyl sulfonate, *FA* formic acid, *WT* wild type

Enhancing hepatic Aβ clearance attenuates AD-type pathologies and behavioral deficits.

To evaluate the therapeutic potential of enhancing the hepatic Aβ clearance for AD, LRP-1 was overexpressed specifically in hepatocytes by genetically delivering exogenous functional LRP-1 minigene to 6-month-old APP/PS1 mice (AD-AAV$_{mLRP-1}$) (Fig. 5a and Supplementary Fig. 6a). Mice were sacrificed and analyzed at 12 months of age. The AD-AAV$_{mLRP-1}$ mice had increased LRP-1 levels in the liver (Fig. 5b, c). No significant differences in sLRP-1, transaminase, and cholesterol were observed between the two groups (Supplementary Fig. 6c–e).

Compared with the AD-AAV$_{eGFP}$ mice, the AD-AAV$_{mLRP-1}$ mice had higher Aβ levels in the liver (Supplementary Fig. 6b) and lower Aβ levels in the blood (Fig. 5d), indicating that the capacity of the liver in clearing circulating Aβ was enhanced in AD-AAV$_{mLRP-1}$ mice. Moreover, the AD-AAV$_{mLRP-1}$ mice had less Aβ plaques (Fig. 5e, f) and lower Aβ levels in the brain (Fig. 5g, h). These findings suggest that enhancing Aβ clearance in the liver can attenuate Aβ pathologies in the brain.

As well, compared with the AD-AAV$_{eGFP}$ mice, the AD-AAV$_{mLRP-1}$ mice had lower tau phosphorylation, neuroinflammation, and neurodegeneration, as reflected by decreased levels of tau phosphorylation at Thr231, astrogliosis, and microgliosis, as well as rescued axonal degeneration and neuronal apoptosis (Supplementary Fig. 6f–l).

In addition, the AD-AAV$_{mLRP-1}$ mice displayed better spatial learning and memory consolidation by a shorter escape latency in the platform trial, more time spent in the target quadrant, and a higher number of platform crossings in the probe trial in the MWM test, as well as better spatial recognition memory as reflected by longer distance in the novel arm in the Y-maze test and rescued anxiety-like behavior by higher rearing numbers in the open-field test (Fig. 5i–m).

Discussion

Our present study provides evidence that the liver physiologically clears circulating Aβ, with approximately 13.9% of Aβ42 and 8.9% of Aβ40 in the blood removed when flowing through the liver once. Consistently, we found that levels of plasma Aβ were increased in patients with liver cirrhosis, suggesting that the liver plays a role in regulating circulating Aβ. The localization of Aβ mainly in hepatocytes in the liver of humans and APP/PS1 mice suggests that hepatocytes are the major cell type of the liver responsible for Aβ clearance.

Does the hepatic Aβ clearance function further impact Aβ levels in the brain? We found that acute reduction of blood flow in the liver via hepatic portal vein ligation resulted in an increase of Aβ in both blood and brain ISF. Further, a decline in hepatic Aβ clearance aggravates the brain Aβ burden in APP/PS1 mice. These findings suggest that the hepatic Aβ clearance from the blood could further regulate Aβ levels in the brain. Consistently, previous studies of ours and others have shown that clearing circulating Aβ could effectively reduce cerebral Aβ burden via hemodialysis, peritoneal dialysis, plasma exchange, enhancing Aβ clearance by the kidney or blood monocytes, etc. [2, 6, 16, 26, 36]. Phase III clinical trials with a peripheral injection of Aβ monoclonal antibodies aducanumab and lecanemab can substantially reduce brain PET Aβ signals in AD patients [3, 37]. All these findings support the peripheral "sink" hypothesis which postulates that central and peripheral pools of Aβ co-exist in equilibrium, and sequestering Aβ in blood could facilitate the efflux of Aβ from the brain [8, 17, 18, 33].

The question of whether a decline in hepatic Aβ clearance is involved in AD development is not clear. A growing number of studies have established a link between impaired hepatic function and cognitive impairment [10, 30, 40, 41]. In addition, abnormal hepatic function, as reflected by an elevated ratio of AST to ALT, was associated with increased Aβ deposition in the brain, AD diagnoses and poor cognitive performance in 1581 older adults from the ADNI cohort [23], suggesting that dysfunctional hepatic clearance may play a role in regulating brain Aβ pathology and AD development. In the present study, we have provided direct experimental evidence showing that chronic decline of Aβ clearance in the liver increased brain Aβ deposition, aggravated tau hyperphosphorylation, neuroinflammation, neurodegeneration, and cognitive deficits in APP/PS1 mice.

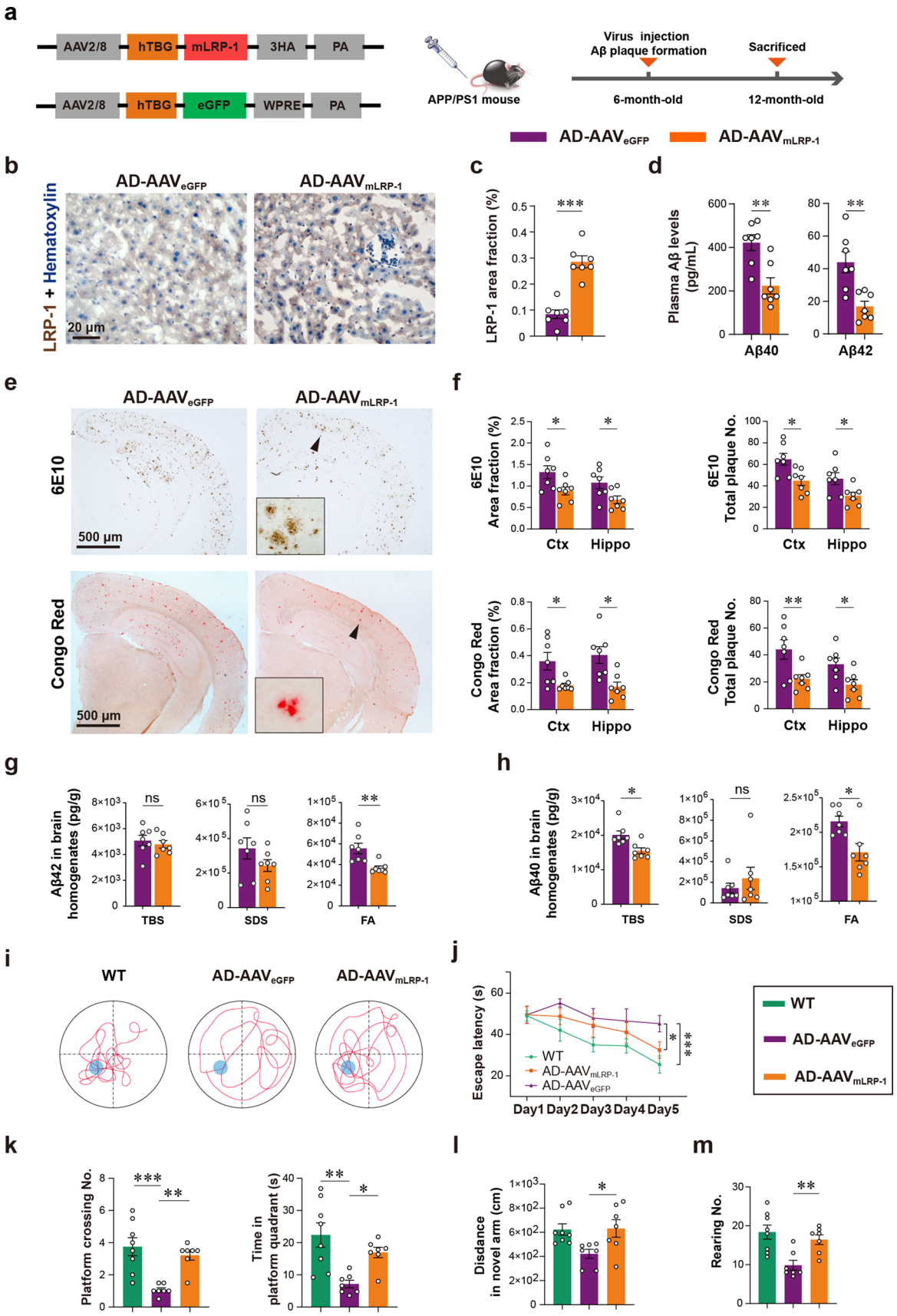
a
AAV2/8
hTBG
mLRP-1
3HA
PA
AAV2/8
hTBG
eGFP
WPRE
PA
APP/PS1 mouse
Virus injection
Aβ plaque formation
Sacrificed
6-month-old
12-month-old
AD-AAVeGFP
AD-AAVmLRP-1
b
AD-AAVeGFP
AD-AAVmLRP-1
LRP-1 + Hematoxylin
20 μm
c
LRP-1 area fraction (%)
d
Plasma Aβ levels (pg/mL)
Aβ40
Aβ42
e
AD-AAVeGFP
AD-AAVmLRP-1
6E10
Congo Red
500 μm
f
6E10 Area fraction (%)
6E10 Total plaque No.
Congo Red Area fraction (%)
Congo Red Total plaque No.
Ctx
Hippo
g
Aβ42 in brain homogenates (pg/g)
TBS
SDS
FA
h
Aβ40 in brain homogenates (pg/g)
TBS
SDS
FA
i
WT
AD-AAVeGFP
AD-AAVmLRP-1
j
Escape latency (s)
Day1 Day2 Day3 Day4 Day5
WT
AD-AAVmLRP-1
AD-AAVeGFP
WT
AD-AAVeGFP
AD-AAVmLRP-1
k
Platform crossing No.
Time in platform quadrant (s)
l
Disdance in novel arm (cm)
m
Rearing No.

◂**Fig. 5** Enhancing the hepatic capacity of Aβ clearance alleviates the Aβ burden and rescues cognitive impairments. **a**–**c** Schematic diagram of liver-specific mLRP-1 expression virus in a model APP/PS1 mouse (virus injection at 6 months of age and analysis at 12 months of age), and the mLRP-1 expression effects, as reflected by immunohistochemical staining with an anti-LRP-1 antibody. **d** Aβ levels in the blood of the AD-AAV$_{mLRP-1}$ and AD-AAV$_{eGFP}$ mice. Unpaired *t* test, $n=7$ per group. **e**, **f** Immunostaining and quantification of Aβ plaques stained with 6E10 and Congo red in the neocortex and hippocampus of 12-month-old AD-AAV$_{mLRP-1}$ and AD-AAV$_{eGFP}$ mice. Unpaired *t* test, $n=7$ per group. **g**, **h** Comparison of Aβ40 and Aβ42 levels in the TBS, SDS, and FA fractions of brain homogenates between the AD-AAV$_{mLRP-1}$ and AD-AAV$_{eGFP}$ mice. Unpaired *t* test, $n=7$ per group. **i**, **j** Water maze tracing graphs and latency from day one to day five. **k** Time spent in the platform quadrant and platform crossing numbers in the target quadrant by WT, AD-AAV$_{mLRP-1}$, and AD-AAV$_{eGFP}$ mice in the Morris water maze. One-way ANOVA, $n=8$ in WT group, $n=7$ in AD-AAV group. **l**, **m** Moving distance and rearing numbers of wild type, AD-AAV$_{mLRP-1}$, and AD-AAV$_{eGFP}$ mice in the open-field test. One-way ANOVA, $n=8$ in WT group, $n=7$ in AD-AAV group. $^{*}p<0.05$, $^{**}p<0.01$, $^{***}p<0.001$. ns denotes no significance. The error bars represent the SEMs. *mLRP-1* minigene LRP-1, *Aβ* amyloid-β protein, *TBS* Tris buffer solution, *SDS* sodium dodecyl sulfonate, *FA* formic acid, *WT* wild type

These findings imply that reduced hepatic Aβ clearance is a potential factor involved in AD development. Whether liver diseases could induce AD pathology in the brain of humans is worth exploring in the future.

Aging is considered the major risk factor for sporadic AD and leads to declined function in all organs of the whole body [13]. We found that the uptake of Aβ42 by the liver decreased with age, along with the reduction in LRP-1 expression in mice. Similarly, a previous study also reported decreased hepatic uptake of ^{125}I-labeled Aβ40 and LRP-1 expression in aged rats [35]. The above studies indicate that aging is an important factor causing declined Aβ clearance by the liver, where the reduction of LRP-1 expression may play an important role. In the present study, plasma Aβ levels increased with age in humans, implying that Aβ clearance is decreased with age in the periphery. Unfortunately, no associations were observed between hepatic function indexes and either age or plasma Aβ levels, implying that current clinically available liver function indexes are not able to reflect liver aging. As mentioned above, liver LRP-1 may be a better marker to reflect the relationship between liver aging and Aβ clearance. This needs to be further verified in humans.

The effects of hepatic Aβ clearance on Aβ levels in the blood and the brain also have implications in the diagnosis and treatment of AD. Some chronic hepatic disorders or diseases (e.g. liver cirrhosis, fatty liver disease, chronic hepatitis, etc.) may lead to increased Aβ levels and potentially result in incorrect or missed diagnosis of AD based on biomarkers. Recent AD biomarker studies found that comorbidities such as chronic kidney disease, myocardial infarction, stroke, etc., significantly affect Aβ and tau levels in the blood and disturb the establishment of a normal reference range and cut points of blood biomarkers for AD [20, 34]. Future biomarker studies on AD diagnosis involving blood Aβ should also take into consideration the effects of chronic hepatic disorders or diseases.

The traditional view on AD drug development believes that therapeutics promoting brain Aβ clearance is required to overcome the obstacle of the blood–brain barrier (BBB) [18]. This view has prevented many potential therapeutics from entering clinical trials. Based on several studies which support the peripheral sink hypothesis, we have proposed to develop AD therapeutic strategies from a systemic approach [39]. In the present study, we found that enhancing hepatic Aβ clearance by upregulating LRP-1 expression in the liver could rescue AD pathologies in the brain and improve cognition in APP/PS1 mice. Consistently, it has been reported that upregulating LRP-1 expression in the liver by *Withania somnifera* attenuated cerebral AD pathologies and cognitive deficits in APP/PS1 mice [27]. These studies suggest that targeting the periphery including the liver may be a promising therapeutic approach for AD. Most importantly, targeting the periphery for Aβ clearance may avoid adverse effects of therapeutics on the brain through BBB.

In conclusion, our findings demonstrate that the liver physiologically clears Aβ from the blood and further regulates Aβ levels in the brain, suggesting that facilitating Aβ clearance via the liver represents a novel potential therapeutic approach for AD. Our study provides a novel insight into the disease pathogenesis, diagnosis, and intervention for AD from a systemic perspective and additional evidence of targeting peripheral Aβ for drug development.

Supplementary Information The online version contains supplementary material available at https://doi.org/10.1007/s00401-023-02559-z.

Acknowledgements We sincerely appreciate Dr. Berislav V. Zlokovic at Zilkha Neurogenetic Institute, University of Southern California, for kindly providing the plasmid information of the LRP-1 minigene. This study was supported by the National Natural Science Foundation of China (No. 81930028 and 31921003).

Author contributions YJW, JW, and YMX conceived and designed the project, YC, GHZ, YYS, HLS, XLB, and HML conducted patient enrollment, assessment and sample treatment, YC, CYH, DYT, SHC, JRR, MYX, DYF, JMJ, PYS, AYS, and WSJ conducted animal and in vitro experiments, YC, CYH, and CRT analyzed data, YC and YJW wrote the manuscript.

Data availability All relevant data generated and analyzed in this study are available in this manuscript, online supplementary information or upon reasonable request.

Declarations

Conflict of interest The authors declare no conflicts of interest.

References

1. Alexander GC, Knopman DS, Emerson SS, Ovbiagele B, Kryscio RJ, Perlmutter JS (2021) Revisiting FDA approval of aducanumab. N Engl J Med 385:769–771. https://doi.org/10.1056/NEJMp2110468
2. Boada M, Lopez OL, Olazaran J, Nunez L, Pfeffer M, Paricio M et al (2020) A randomized, controlled clinical trial of plasma exchange with albumin replacement for Alzheimer's disease: primary results of the AMBAR Study. Alzheimers Dement 16:1412–1425. https://doi.org/10.1002/alz.12137
3. Budd Haeberlein S, Aisen PS, Barkhof F, Chalkias S, Chen T, Cohen S et al (2022) Two randomized phase 3 studies of aducanumab in early Alzheimer's disease. J Prev Alzheimers Dis 9:197–210. https://doi.org/10.14283/jpad.2022.30
4. Carlisle KM, Halliwell M, Read AE, Wells PN (1992) Estimation of total hepatic blood flow by duplex ultrasound. Gut 33:92–97. https://doi.org/10.1136/gut.33.1.92
5. Charni-Natan M, Goldstein I (2020) Protocol for primary mouse hepatocyte isolation. STAR Protoc. 1:100086. https://doi.org/10.1016/j.xpro.2020.100086
6. Chen SH, He CY, Shen YY, Zeng GH, Tian DY, Cheng Y et al (2022) Polysaccharide krestin prevents Alzheimer's disease-type pathology and cognitive deficits by enhancing monocyte amyloid-beta processing. Neurosci Bull 38:290–302. https://doi.org/10.1007/s12264-021-00779-5
7. Coleridge JC, Hemingway A (1958) Partition of the venous return of the heart. J Physiol 142:366–381. https://doi.org/10.1113/jphysiol.1958.sp006023
8. DeMattos RB, Bales KR, Cummins DJ, Dodart JC, Paul SM, Holtzman DM (2001) Peripheral anti-A beta antibody alters CNS and plasma A beta clearance and decreases brain A beta burden in a mouse model of Alzheimer's disease. Proc Natl Acad Sci U S A 98:8850–8855
9. Estrada LD, Ahumada P, Cabrera D, Arab JP (2019) Liver dysfunction as a novel player in Alzheimer's progression: Looking outside the brain. Front. Aging Neurosci. 11:174. https://doi.org/10.3389/fnagi.2019.00174
10. Filipovic B, Markovic O, Duric V, Filipovic B (2018) Cognitive changes and brain volume reduction in patients with nonalcoholic fatty liver disease. Can J Gastroenterol Hepatol 2018:9638797. https://doi.org/10.1155/2018/9638797
11. Ghiso J, Shayo M, Calero M, Ng D, Tomidokoro Y, Gandy S et al (2004) Systemic catabolism of Alzheimer's Abeta40 and Abeta42. J Biol Chem 279:45897–45908. https://doi.org/10.1074/jbc.M407668200
12. Hardy JA, Higgins GA (1992) Alzheimer's disease: the amyloid cascade hypothesis. Science 256:184–185. https://doi.org/10.1126/science.1566067
13. Hou Y, Dan X, Babbar M, Wei Y, Hasselbalch SG, Croteau DL et al (2019) Ageing as a risk factor for neurodegenerative disease. Nat Rev Neurol 15:565–581. https://doi.org/10.1038/s41582-019-0244-7
14. Huang Y, Mucke L (2012) Alzheimer mechanisms and therapeutic strategies. Cell 148:1204–1222. https://doi.org/10.1016/j.cell.2012.02.040
15. Jansen IE, Savage JE, Watanabe K, Bryois J, Williams DM, Steinberg S et al (2019) Genome-wide meta-analysis identifies new loci and functional pathways influencing Alzheimer's disease risk. Nat Genet 51:404–413. https://doi.org/10.1038/s41588-018-0311-9
16. Jin WS, Shen LL, Bu XL, Zhang WW, Chen SH, Huang ZL et al (2017) Peritoneal dialysis reduces amyloid-beta plasma levels in humans and attenuates Alzheimer-associated phenotypes in an APP/PS1 mouse model. Acta Neuropathol 134:207–220. https://doi.org/10.1007/s00401-017-1721-y
17. Lemere CA, Spooner ET, LaFrancois J, Malester B, Mori C, Leverone JF et al (2003) Evidence for peripheral clearance of cerebral Abeta protein following chronic, active Abeta immunization in PSAPP mice. Neurobiol Dis 14:10–18. https://doi.org/10.1016/s0969-9961(03)00044-5
18. Liu YH, Giunta B, Zhou HD, Tan J, Wang YJ (2012) Immunotherapy for Alzheimer disease: the challenge of adverse effects. Nat Rev Neurol 8:465–469. https://doi.org/10.1038/nrneurol.2012.118
19. Macauley SL, Stanley M, Caesar EE, Yamada SA, Raichle ME, Perez R et al (2015) Hyperglycemia modulates extracellular amyloid-beta concentrations and neuronal activity in vivo. J Clin Investig 125:2463–2467. https://doi.org/10.1172/JCI79742
20. Mielke MM, Dage JL, Frank RD, Algeciras-Schimnich A, Knopman DS, Lowe VJ et al (2022) Performance of plasma phosphorylated tau 181 and 217 in the community. Nat Med 28:1398–1405. https://doi.org/10.1038/s41591-022-01822-2
21. Mohar I, Brempelis KJ, Murray SA, Ebrahimkhani MR, Crispe IN (2015) Isolation of non-parenchymal cells from the mouse liver. Methods Mol Biol 1325:3–17. https://doi.org/10.1007/978-1-4939-2815-6_1
22. Newton JL, Hollingsworth KG, Taylor R, El-Sharkawy AM, Khan ZU, Pearce R et al (2008) Cognitive impairment in primary biliary cirrhosis: symptom impact and potential etiology. Hepatology 48:541–549. https://doi.org/10.1002/hep.22371
23. Nho K, Kueider-Paisley A, Ahmad S, MahmoudianDehkordi S, Arnold M, Risacher SL et al (2019) Association of altered liver enzymes with Alzheimer disease diagnosis, cognition, neuroimaging measures, and cerebrospinal fluid biomarkers. JAMA Netw Open 2:e197978. https://doi.org/10.1001/jamanetworkopen.2019.7978
24. Nikolakopoulou AM, Wang Y, Ma Q, Sagare AP, Montagne A, Huuskonen MT et al (2021) Endothelial LRP1 protects against neurodegeneration by blocking cyclophilin A. J Exp Med. https://doi.org/10.1084/jem.20202207
25. Qosa H, Abuasal BS, Romero IA, Weksler B, Couraud PO, Keller JN et al (2014) Differences in amyloid-beta clearance across mouse and human blood-brain barrier models: kinetic analysis and mechanistic modeling. Neuropharmacology 79:668–678. https://doi.org/10.1016/j.neuropharm.2014.01.023
26. Sakai K, Senda T, Hata R, Kuroda M, Hasegawa M, Kato M et al (2016) Patients that have undergone hemodialysis exhibit lower amyloid deposition in the brain: evidence supporting a therapeutic strategy for Alzheimer's disease by removal of blood amyloid. J Alzheimers Dis 51:997–1002. https://doi.org/10.3233/JAD-151139
27. Sehgal N, Gupta A, Valli RK, Joshi SD, Mills JT, Hamel E et al (2012) *Withania somnifera* reverses Alzheimer's disease pathology by enhancing low-density lipoprotein receptor-related protein in liver. Proc Natl Acad Sci U S A 109:3510–3515. https://doi.org/10.1073/pnas.1112209109
28. Selkoe DJ (1999) Translating cell biology into therapeutic advances in Alzheimer's disease. Nature 399:A23-31. https://doi.org/10.1038/399a023
29. Selkoe DJ, Hardy J (2016) The amyloid hypothesis of Alzheimer's disease at 25 years. EMBO Mol Med 8:595–608. https://doi.org/10.15252/emmm.201606210
30. Seo SW, Gottesman RF, Clark JM, Hernaez R, Chang Y, Kim C et al (2016) Nonalcoholic fatty liver disease is associated with cognitive function in adults. Neurology 86:1136–1142. https://doi.org/10.1212/WNL.0000000000002498
31. Severgnini M, Sherman J, Sehgal A, Jayaprakash NK, Aubin J, Wang G et al (2012) A rapid two-step method for isolation of functional primary mouse hepatocytes: cell characterization and asialoglycoprotein receptor based assay development. Cytotechnology 64:187–195. https://doi.org/10.1007/s10616-011-9407-0

32. Shinohara M, Tachibana M, Kanekiyo T, Bu G (2017) Role of LRP1 in the pathogenesis of Alzheimer's disease: evidence from clinical and preclinical studies. J Lipid Res 58:1267–1281. https://doi.org/10.1194/jlr.R075796
33. Sigurdsson EM, Knudsen E, Asuni A, Fitzer-Attas C, Sage D, Quartermain D et al (2004) An attenuated immune response is sufficient to enhance cognition in an Alzheimer's disease mouse model immunized with amyloid-beta derivatives. J Neurosci 24:6277–6282. https://doi.org/10.1523/JNEUROSCI.1344-04.2004
34. Syrjanen JA, Campbell MR, Algeciras-Schimnich A, Vemuri P, Graff-Radford J, Machulda MM et al (2022) Associations of amyloid and neurodegeneration plasma biomarkers with comorbidities. Alzheimers Dement 18:1128–1140. https://doi.org/10.1002/alz.12466
35. Tamaki C, Ohtsuki S, Iwatsubo T, Hashimoto T, Yamada K, Yabuki C et al (2006) Major involvement of low-density lipoprotein receptor-related protein 1 in the clearance of plasma free amyloid beta-peptide by the liver. Pharm Res 23:1407–1416. https://doi.org/10.1007/s11095-006-0208-7
36. Tian DY, Cheng Y, Zhuang ZQ, He CY, Pan QG, Tang MZ et al (2021) Physiological clearance of amyloid-beta by the kidney and its therapeutic potential for Alzheimer's disease. Mol Psychiatry 26:6074–6082. https://doi.org/10.1038/s41380-021-01073-6
37. van Dyck CH, Swanson CJ, Aisen P, Bateman RJ, Chen C, Gee M et al (2022) Lecanemab in early Alzheimer's disease. N Engl J Med. https://doi.org/10.1056/NEJMoa2212948
38. van Dyck CH, Swanson CJ, Aisen P, Bateman RJ, Chen C, Gee M et al (2023) Lecanemab in early Alzheimer's disease. N Engl J Med 388:9–21. https://doi.org/10.1056/NEJMoa2212948
39. Wang J, Gu BJ, Masters CL, Wang YJ (2017) A systemic view of Alzheimer disease—insights from amyloid-beta metabolism beyond the brain. Nat Rev Neurol 13:612–623. https://doi.org/10.1038/nrneurol.2017.111
40. Weinstein G, Davis-Plourde K, Himali JJ, Zelber-Sagi S, Beiser AS, Seshadri S (2019) Non-alcoholic fatty liver disease, liver fibrosis score and cognitive function in middle-aged adults: the Framingham study. Liver Int 39:1713–1721. https://doi.org/10.1111/liv.14161
41. Weinstein G, Zelber-Sagi S, Preis SR, Beiser AS, DeCarli C, Speliotes EK et al (2018) Association of nonalcoholic fatty liver disease with lower brain volume in healthy middle-aged adults in the Framingham Study. JAMA Neurol 75:97–104. https://doi.org/10.1001/jamaneurol.2017.3229
42. Xiang Y, Bu XL, Liu YH, Zhu C, Shen LL, Jiao SS et al (2015) Physiological amyloid-beta clearance in the periphery and its therapeutic potential for Alzheimer's disease. Acta Neuropathol 130:487–499. https://doi.org/10.1007/s00401-015-1477-1
43. Yang C, Liu ZL, Wang J, Bu XL, Wang YJ, Xiang Y (2021) Parabiosis modeling: protocol, application and perspectives. Zool Res 42:253–261. https://doi.org/10.24272/j.issn.2095-8137.2020.368
44. Yao XQ, Jiao SS, Saadipour K, Zeng F, Wang QH, Zhu C et al (2015) p75NTR ectodomain is a physiological neuroprotective molecule against amyloid-beta toxicity in the brain of Alzheimer's disease. Mol Psychiatry 20:1301–1310. https://doi.org/10.1038/mp.2015.49